Chapter 1

Promises and Pitfalls of Polarimetry

1.1 Introduction

Imagine an observational technique, differential in nature, that takes full advantage of the information content a photon has to offer. Photometric conditions would be unecessary, allowing ground-based telescopes to outsrip their space-based counterparts for uses where imaging is not required. Indeed, such a technique has been around for decades in the form of polarimetry. Why, then, are the numbers of polarimeters and polarimetrists so few? Does the bright side of polarimetry simply fall on blind eyes?

In 1852, Sir George Gabriel Stokes invented a formalism for decomposing the electric field oscillations of light that is still used today. Consider a right-handed, Cartesian coordinate system with light propagating in the $\hat{z}$ direction. The electric field of this light beam varies in time as

$$\vec{E}(t) = E_x \cos(\omega t - \delta_x)\hat{x} + E_y \cos(\omega t - \delta_y)\hat{y} \tag{1.1}$$

with amplitudes and phases E_i and δ_i. The path of the electric field vector, when projected onto the xy plane, describes an ellipse. Such light is therefore "elliptically polarized".

The Stokes parameters I, Q, U, and V are defined by the time-averaged quantities

$$I = \left\langle E_x^2 \right\rangle + \left\langle E_y^2 \right\rangle \tag{1.2a}$$

$$Q = \left\langle E_x^2 \right\rangle - \left\langle E_y^2 \right\rangle \tag{1.2b}$$

$$U = 2 \left\langle E_x E_y \cos(\delta_x - \delta_y) \right\rangle \tag{1.2c}$$

$$V = 2 \left\langle E_x E_y \sin(\delta_x - \delta_y) \right\rangle . \tag{1.2d}$$

Thus, the Stokes I parameter describes the total intensity of the beam. Stokes Q and U are measures of the "linear" polarization of the light beam, where Stokes Q represents the net electric field component along the $\hat{x}$ ($+Q$) or $\hat{y}$ ($-Q$) direction and Stokes $\pm U$ describes the net electric field component at $\pm 45°$ from the $\hat{x}$ direction. Stokes V, a measure of the "circular" polarization of the light beam, represents the net electric field component that rotates clockwise ($+V$) or counterclockwise ($-V$) at constant angular frequency.

The orthogonal basis vectors of linear polarization, Q and U, are only separated by 45° in physical space. Rotation of a light beam by $\pm 90°$ reverses the sign of Q and U. Therefore, periodicity in linear polarization occurs by rotation through 180°. When projected onto the sky, Stokes $+Q$ points north/south, $-Q$ east/west, $+U$ northeast/southwest, and $-U$ is northwest/southeast (Figure 1.1). Stokes parameters are usually normalized to the intensity of light, I. The fractional degree and position angle of net polarization are then

$$P \equiv \sqrt{\left(\frac{Q}{I}\right)^2 + \left(\frac{U}{I}\right)^2 + \left(\frac{V}{I}\right)^2} \tag{1.3a}$$

$$\Theta \equiv \frac{1}{2} \arctan \frac{U/I}{Q/I} . \tag{1.3b}$$

Polarimetry is therefore a differential technique, where the *fractional* degree of polarized light and its orientation are the relevant quantities. This is in contrast to absolute techniques such as photometry, which require stringent calibration to determine whether fluctuations in data are intrinsic to the source or are due to systematic effects.

To utilize photometry as a differential technique, one must monitor photometric standard stars

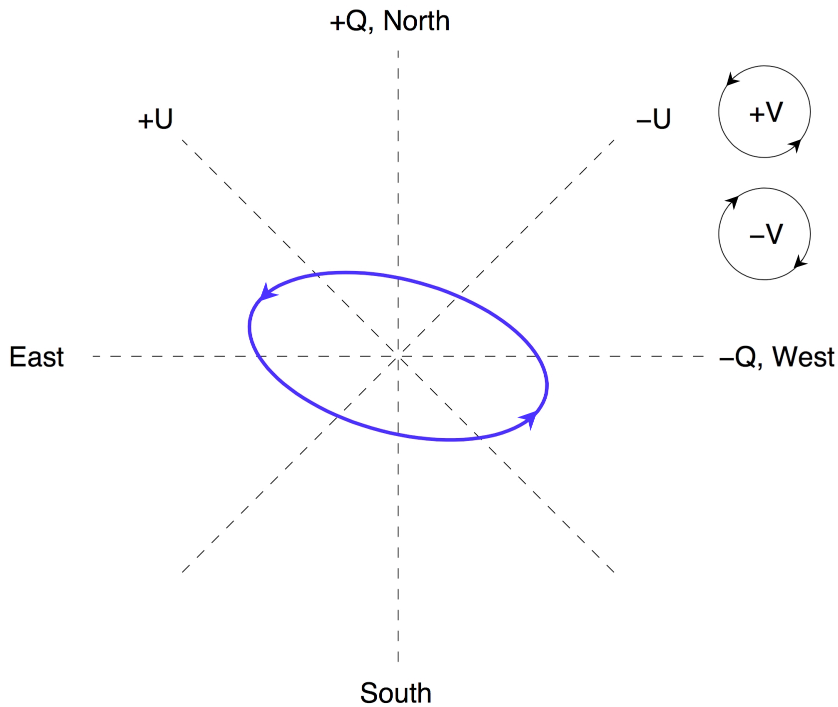

Figure 1.1: Stokes parameters projected onto the sky. The ellipse indicates a general, elliptically polarized light beam with Stokes parameters $-Q$, $+U$, and $+V$, where $Q > U$.

simultaneously with the target. The non-uniformity of the Earth's atmosphere forces one to choose standard stars at a small angular distance from the target. Thus, if a pocket of turbulence passes through the line of sight of both stars roughly simultaneously, the scintillation event should be subtracted out. Even for high quality calibration, however, photometric precision better than one part in 10^3 is extremely difficult to achieve from the ground. Space-based telescopes overcome scintillation from the atmosphere, but their smaller apertures ensure that even photon shot noise-limited operation rarely produces precision less than one part in 10^4. However, I will show in subsequent chapters that I have achieved polarimetric precision on bright stars of order one part per million.

Unfortunately, polarimetry still requires calibration. The largest source of uncertainty in polarimetric measurements is usually polarization intrinsic to the telescope and instrument. Polarization of light is sensitive to the geometry of scattering as well as the optical properties of the scatterer. Therefore, asymmetries in mirror coating, as well as asymmetry in the angle of reflection integrated over the mirror surface, will generate intrinsic polarization. Analogous to dark subtraction in photometry, subtraction of this telescope/instrument polarization is required. Generally this progresses by observing "unpolarized" standard stars. Since polarization is sensitive to asymmetry in the source, nothing in the Universe is truly unpolarized. However, it is possible to measure polarization consistent with zero for some stars. Sky subtraction proceeds identically in polarimetry as it does in photometry, and conventional flat-fielding is required in imaging polarimetry. In addition, polarized standard stars are observed to ensure that the gain of the system is calibrated. This is effectively flat-fielding for single-pixel detectors. Since appropriate calibration can indeed be performed, what are the benefits of observing polarized light from the sky?

1.2 Promises of Polarimetry

1.2.1 Extrasolar Planets

Extrasolar planets are one of the most exciting objects in astronomy to study. Questions such as "How did we get here?" and "Are we alone?" are directly applicable to the study of extrasolar planets. Regarding the former question, planet formation is the result of accretion of material in circumstellar disks. Polarimetry can provide valuable clues to the nuances of this process and will be discussed later. As for the latter question, the existence of planets around other stars has been sought since recorded history. Evidence of Earth-like, or at least life-supporting, planets could have enormous impact on virtually all aspects of society, not the least of which would be the impact on planning and funding future astronomical investigations.

The first extrasolar planets were discovered around a pulsar in 1992 by observing periodic Doppler shifts in its pulses (Wolszczan & Frail 1992). These three nearly Earth-mass planets have masses 0.020 ± 0.002, 4.3 ± 0.2, and 3.9 ± 0.2 $M_{\oplus}$ and orbit PSR B1257+12 with periods of $\approx$ 25, 67, and 98 days, respectively (Konacki & Wolszczan 2003). Beginning in 1995, hundreds of close-in, Jupiter-mass planets have been detected by periodicities in stellar radial velocity (Mayor & Queloz 1995). Recently, extrasolar planet research has progressed from planet detection to the beginning stages of planet characterization. Infrared planetary emission has been directly detected (Deming et al. 2005), and dayside/nightside contrast in that emission has been observed (Knutson et al. 2007). Moreover, while the initial detected population of extrasolar planets was of order one Jupiter mass, refinement of the radial velocity technique has permitted Neptune-mass planets to be discovered (Lovis et al. 2006).

However, to truly begin to characterize individual planets, their most basic characteristic, mass, must be accurately determined. Since the radial velocity technique is insensitive to stellar reflex motion in the plane of the sky, estimation of precise masses for the large majority of known planets is hampered by the inability to measure orbital inclination, i. Measured mass, m, is only a lower limit to the true mass, M, because $m = M \sin i$. Planets in edge-on orbits transit the disk of their host star every orbit, which causes a periodic dip in the stellar flux as the planet transits the disk of its parent star. The shape of the system lightcurve is indicative of orbital inclination, so inclination estimates from transit observations can be coupled with radial velocity data to derive accurate masses. Indeed, masses of transiting planets can be measured with a precision of less than one Jupiter mass. The transit of HD 209458 was discovered by Charbonneau et al. (2000); since then, dozens of transiting planets have been discovered. However, the probability of transit occurrence in a sample of systems with randomly distributed inclinations scales as R_*/a, where R_* is the stellar radius and a is the planetary semimajor axis. This is because the solid angle subtended by the transit shadow is $2\pi \times 2R_*/a$ out of a total 4π steradians. Thus, transiting planets only comprise $\approx 10\%$ of known extrasolar planets.

Astrometry holds promise for determining masses of planets, because the star's motion in the plane of the sky is observed. The astrometric motion a_* of an extrasolar planet host star is simply the star's lever arm with respect to the center of mass of the system:

$$a_* = a \left(\frac{M_p}{M_*} \right). \tag{1.4}$$

Since typical mass ratios for extrasolar planets/host stars are of order one part in 10^{-3}, the astrometric motion of a star 100 parsecs away with a planet at $a = 0.05$ AU is of order 0.5 μas. While space-based interferometers have the potential to graze this regime, astrometric mass measurements are more likely for planets at larger semimajor axes. The same selection effect occurs for direct imaging of planetary emission, because a star's diffracted halo decreases in brightness with increase in angular distance. Therefore, orbits of extrasolar planets seen astrometrically or by direct imaging are more likely for planets at large semimajor axes.

This differs from the radial velocity technique, because close-in extrasolar planets are preferentially selected for because of two reasons. First, stellar velocities scale as

$$v = \frac{2\pi a}{T} = \frac{2\pi}{\sqrt{a}} \tag{1.5}$$

for circular orbits, where a is orbital semimajor axis. Second, close-in planets undergo more orbits in a given amount of time than do planets at larger semimajor axes, so confirmation of statistically significant periodicity requires a shorter temporal baseline.

We are developing an observational technique that has the potential to determine system inclination for close-in extrasolar planets (so-called "hot Jupiters"). System inclination, and therefore unambiguous mass, can be found by monitoring the polarization of the system throughout its orbit. Polarization of hot Jupiters arises by scattering of incident starlight by gas molecules, aerosols, and dust grains in the planet's atmosphere. For a face-on orbit (Figure 1.2a), the planet is always seen at quadrature and will always have half of its disk illuminated. Since the intensity of light scattered by the planet is constant throughout the orbit, the degree of polarization will also be constant.

However, the position angle of polarization will rotate through 360° each orbit. This is because the position angle from single scattering events is perpendicular to the plane containing the light source, the scatterer, and the observer (i.e., the scattering plane). In contrast, an edge-on viewing geometry will generate large, periodic variability in the degree of polarization (Figure 1.2b). For this geometry, the planet will appear to go through the complete cycle of full to new phases, just like the Moon. However, the scattering plane will always lie in the plane of the orbit, so the position angle of net polarization will not vary during the orbit. In general, a hot Jupiter system will exhibit variability in the polarization vector that is indicative of orbital inclination.

Hot Jupiters have orbital periods of a few days, so they intercept about one part in 10^5 of their parent star's flux. Disk-integrated polarization of Jupiter itself is of order one percent (Hall & Riley 1976), and spatially resolved polarization of comparable magnitude has been observed on Uranus and Neptune (Figure 1.3). Therefore, the precision required to detect hot Jupiters is one part per million to one part in ten million of the star's total flux. The polarization of the host star itself is at the level of one part in 10^4 or lower and is primarily due to interstellar extinction. Since the planet's orbital frequency is known to high precision from radial velocity, stellar polarization and its variability can be separated from the planetary signal.

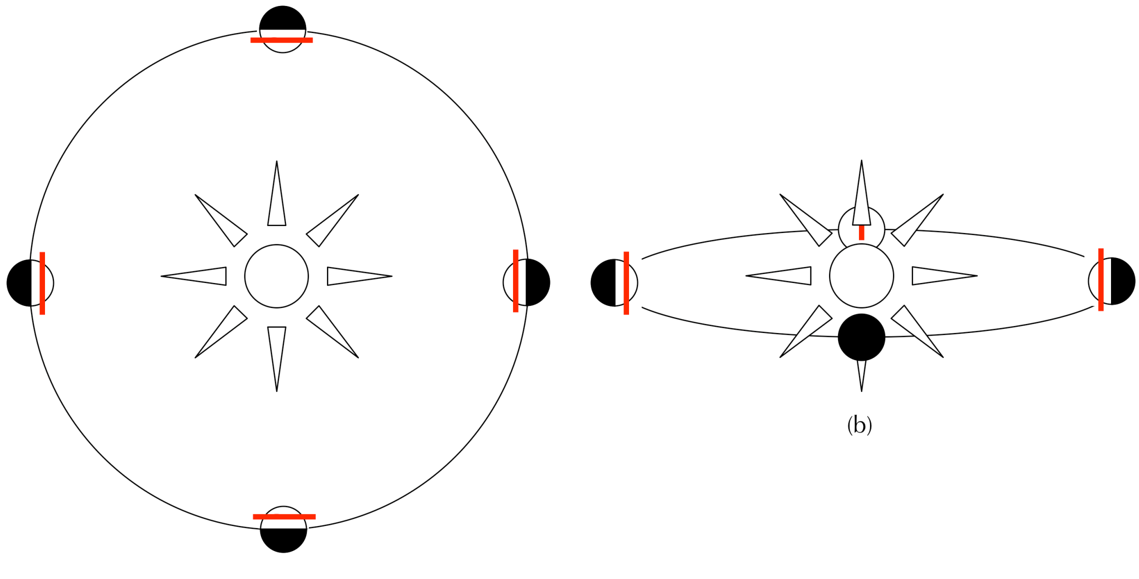

Figure 1.2: Theoretical orbital modulation of system polarization for a hot Jupiter system. The degree of polarization is represented by the white, illuminated portion of the planet. The position angle of net polarization is given by the orientation of the red lines. The face-on case is shown in (a), and the edge-on case is shown in (b).

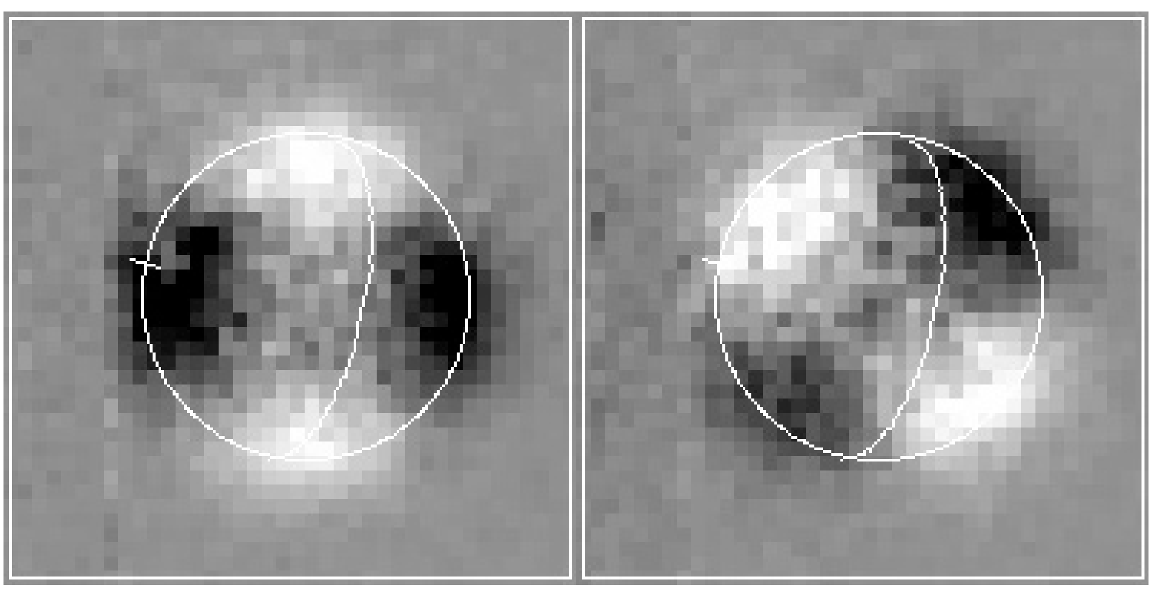

Figure 1.3: Imaging polarimetry of Uranus. This figure is taken from Figure 2 of Schmid et al. (2006). The left image is Stokes Q/I and the right is U/I. Black pixels indicate polarization of -0.5%, and white pixels have polarization of $+0.5\%$. North is up, east is to the left, and the disk of the planet, South Pole, and Equator are outlined in white.

The precision required to observe the modulation in polarization due to the hot Jupiter is one to two orders of magnitude more stringent than the modulation in photometry of the system. However, ground-based photometric observation alone cannot achieve this high precision due to the difficulty in achieving such stringent calibration. Even if the requisite calibration were attained, perhaps from space-based observatories, the low information content from photometry would preclude estimation of system inclination. Polarization is a vector quantity, containing both degree of polarization as well as position angle, while photometry is a scalar quantity. The added information content per photon from polarimetry allows inclinations to be determined. Figure 1.4 (taken from the models of Stam et al. 2004) demonstrates that the amplitude of orbital modulation in polarization of a hot Jupiter is dependent on system inclination. The frequency of polarization modulation is the second harmonic of the orbital frequency because polarization follows a $\cos(2\theta)$ profile through rotation. That is, polarimetric position angles θ and $\theta + 180^\circ$ are identical.

In addition to constraining system inclination (and therefore mass) of extrasolar planets, polarization of these planets can yield information about the atmospheric structure. Calculations of Stam et al. (2004) suggest that both the total reflected flux spectrum and the degree of polarization versus wavelength should be different depending on whether the atmosphere is clear, has cloud layers, or has both cloud and haze layers (Figure 1.5). The maximum polarization of the planet through its orbit will be dependent on the existence or lack of these layers (Figure 1.6b) while the minimum polarization of the planet is dependent on the system inclination (Figure 1.4).

Polarimetry also has the potential to determine the stellar hemisphere transited by an extrasolar planet. This is because the asymmetry in stellar polarization caused by a transiting planet will be reversed between transit ingress and egress. This causes a rotation of the position angle of net polarization of the system throughout the transit, and the sign of rotation on the sky is indicative of the hemisphere that is transited. That is, the position angle of net polarization during a Northern Hemisphere ingress is the same as the position angle during a Southern Hemisphere egress, and vice versa. I will present tentative observations of a transit of the HD 189733 system in Chapter 3.

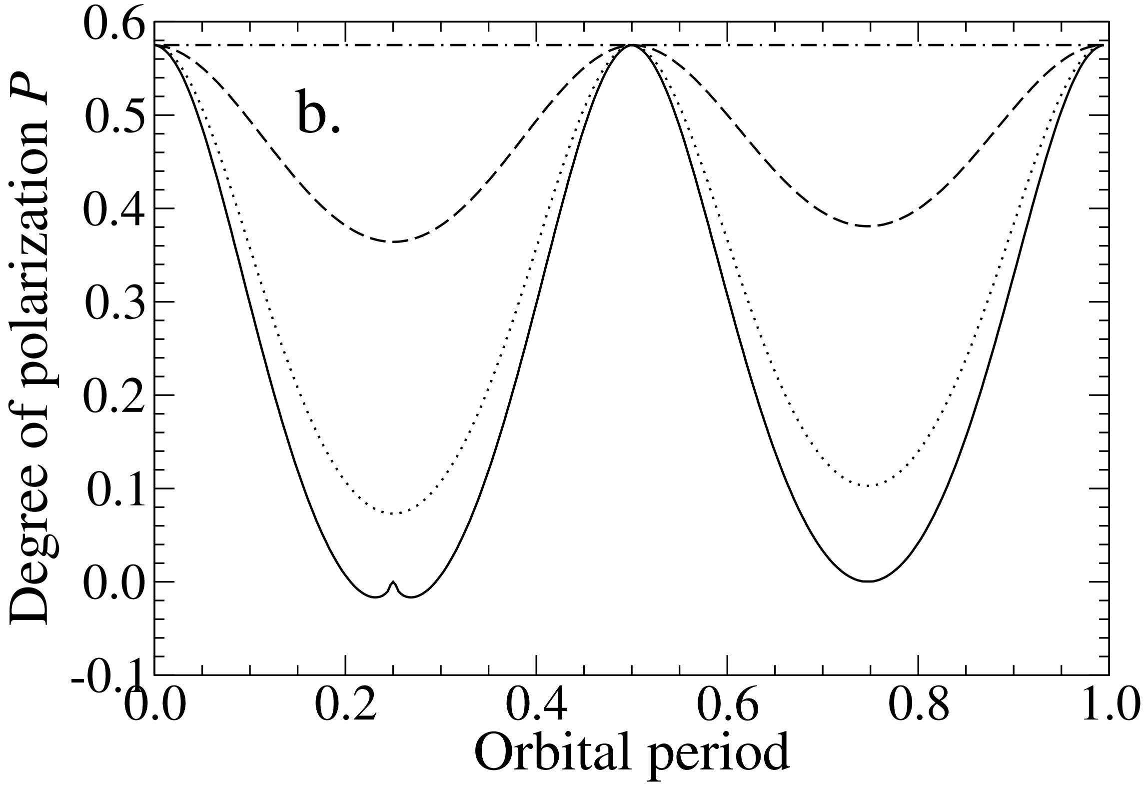

Figure 1.4: Modeled orbital modulation of polarization of a hot Jupiter, given as Figure 7b from Stam et al. (2004). The dot-dashed, dashed, dotted, and solid lines represent inclinations of 0° (face-on), 30°, 60°, and 90° (edge-on), respectively.

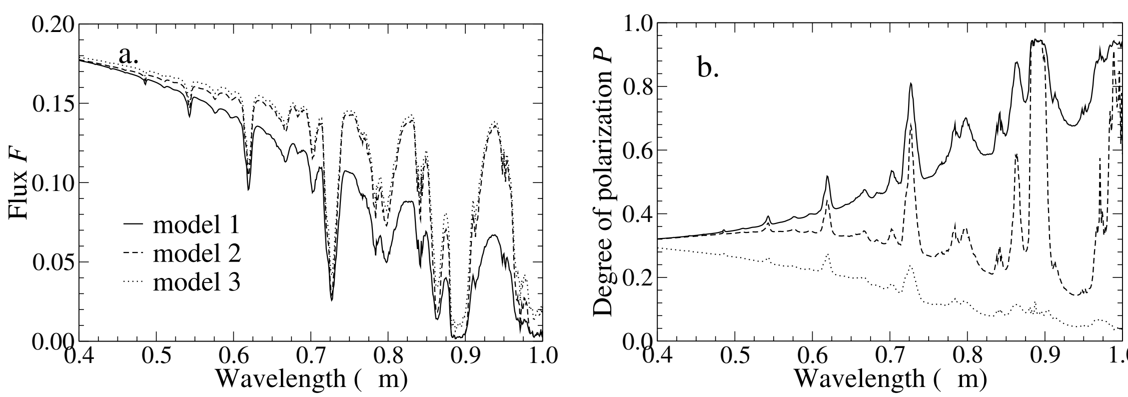

Figure 1.5: (a) Spectrum of scattered flux from a hot Jupiter. (b) Polarized spectrum of a hot Jupiter, taken from Figure 4 of Stam et al. (2004). Models 1, 2, and 3 are for a clear atmosphere, for an atmosphere with a tropospheric cloud layer, and for an atmosphere with both a tropospheric cloud layer and a stratospheric haze layer, respectively. It can be seen that absorption bands are more strongly polarized than the continuum.

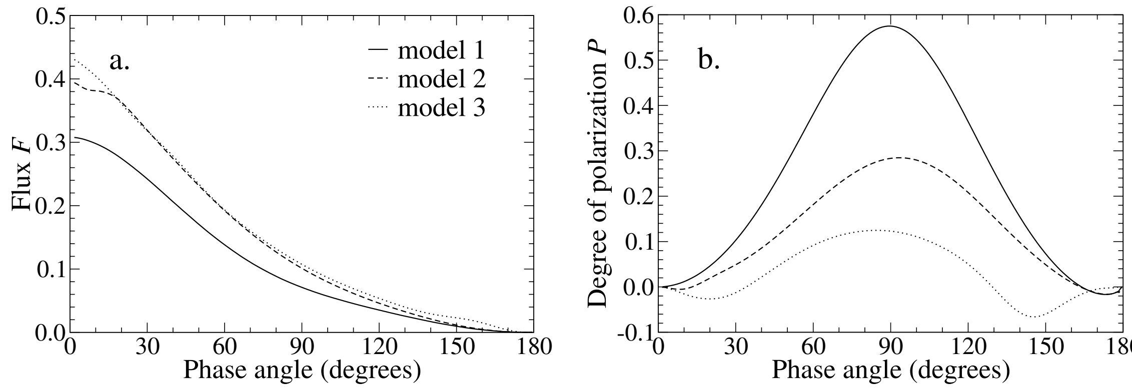

Figure 1.6: (a) Scattered flux and (b) polarization of a hot Jupiter through orbit, taken from Figure 5 of Stam et al. (2004). Existence of clouds and haze can be deduced from the maximum planetary polarization over the orbit.

1.2.2 Black Holes and Neutron Stars

Orbital inclination of high mass X-ray binaries, consisting of an OB supergiant and either a black hole or neutron star, may also be determined from polarimetric monitoring. While the mechanism generating net polarization of the system is different for hot Jupiters and X-ray binaries, phase-locked modulation can give an estimate of inclination. The hot photosphere of the supergiant in such a binary generates significant free electrons which Thomson scatter the stellar flux. Tidal distortion of such a circumbinary envelope, as well as of the supergiant itself, imparts an asymmetry to the system which causes polarimetric modulation. For rigidly rotating, static structure, this modulation occurs at the orbital frequency and first harmonic. Thus, spurious variability at other frequencies can, in principle, be filtered out.

Once the inclination of the system is known, radial velocity data can then provide accurate masses of the compact object, assuming the mass of the supergiant is known. Evolutionary modeling of progenitor stars would greatly benefit from a large sample of known black hole and neutron star masses.

1.2.3 Circumstellar Disks

Vink et al. (2005) observe polarization of seven T Tauri and Herbig Ae/Be objects. They find the position angle of polarization of three objects to be consistent with the position angle of the disk major axis from near-IR interferometric imaging. The remaining four objects have polarimetric position angle $\approx 90^\circ$ from the position angle of the major axis. They interpret these results in terms of single or multiple scattering by optically thin or thick disks, respectively. They also observe a change in degree of polarization versus wavelength across the Hα line. This is interpreted as scattering of starlight by a rotating accretion disk, because the strongest degree of polarization is expected for scattering through 90°. This occurs for material at quadrature phase, which will be moving almost entirely along the line of sight. This material will therefore lie at the Doppler shifted wings of the line.

Nearly edge-on disks of UX Ori objects show increased polarization during times of photometric minima. This is interpreted in terms of dust clumps partially occulting the central star, while light scattered and polarized by the disk is unaffected. Since the amount of polarized light stays roughly constant, while the amount of unpolarized light decreases, the degree of polarization during these occultations increases (Grinin 1994, Grinin et al. 1994, Oudmaijer et al. 2001).

Graham et al. (2007) observe polarization perpendicular to the edge-on disk around AU Mic, which indicates single scattering in an optically thin disk composed of micron sized particles.

1.2.4 Evolved Stars

The process by which nearly spherical stars generate planetary nebulae of strongly asymmetric shape is poorly known. González Delgado et al. (2003) observe a polarized shell of material around the carbon stars R Scl and U Ant (Figure 1.7). Polarimetric modulation of post-AGB stars can be partly explained by non-radial pulsations (Henson et al. 1985, Magalhães et al. 1986, Raveendran & Rao 1989, Yudin & Evans 2002), which may play a role in the production of non-spherical planetary nebulae. Trammell et al. (1994) observed 31 post-AGB stars, and they claim 75% of the sample shows evidence for intrinsic polarization. They take this to be evidence for asphericity in the system. In addition, they observe polarimetric variability which is interpreted as mass loss in the form of clumps. Johnson & Jones (1991) and Bieging et al. (2006) find a positive correlation between evolved star mass loss rate and net polarization (Figure 1.8).

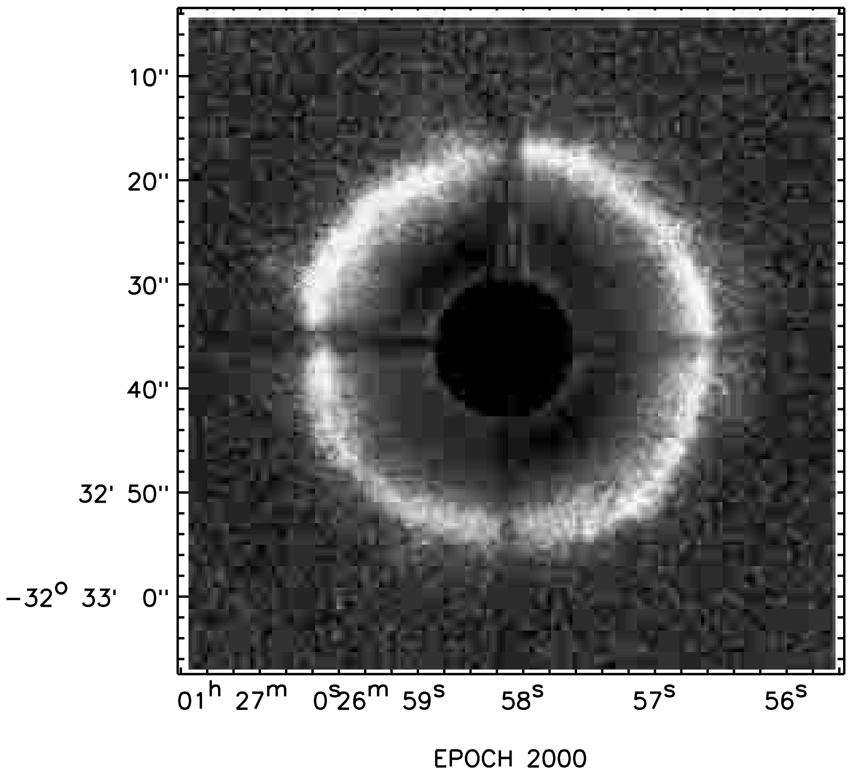

Figure 1.7: Imaging polarimetry of R Scl from Figure 1 of González Delgado et al. (2003).

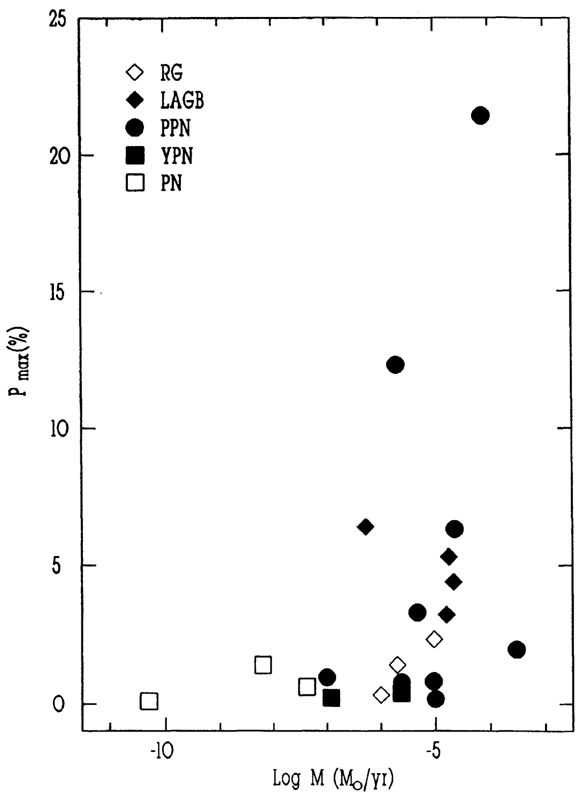

Figure 1.8: Correlation of net polarization and mass loss rate for evolved stars. This figure comes from Figure 3 of Johnson & Jones (1991) and is reproduced by permission of the AAS.

1.3 Pitfalls of Polarimetry

1.3.1 Telescope Polarization

The largest systematic effect in high precision polarimetry is usually telescope and instrument polarization. It is generally present at less than one part in 10^4, which is below the noise floor for imaging polarimetry. However, observations of polarimetry in integrated light, which are necessary in order to reach precisions required for extrasolar planet and other high precision observations, must calibrate telescope polarization. The procedure generally involves observing with an altitude-azimuth telescope with the field de-rotator disabled. Stars thought to be unpolarized, and consequently non-variable on a night-to-night timescale, are observed through a range of parallactic angles. Such stars are generally nearby, so the effect of interstellar polarization is minimized (section 1.3.2). Since telescope polarization dominates the signal, the modulation of observed polarization as the Earth rotates gives a measure of the telescope polarization (Figure 1.9). However, this process is very time consuming, and it must be performed each night. Indeed, Hough et al. (2006b) estimate 20% of observing time is taken up by telescope polarization calibration.

For equatorial mount telescopes, such as the Hale 5-m, one must observe net polarization of stars that are known to exhibit intrinsic plus interstellar polarization that is consistent with zero. This requires identification of such stars from previous, high precision polarimetric investigations on alt-az telescopes. We therefore consult Hough et al. (2006b) for such zero polarization standard stars observed with the PlanetPol instrument.

1.3.2 Interstellar Polarization

Alignment of interstellar dust grains by the galactic magnetic field causes preferential extinction of the electric field component of background starlight parallel to the long axis of the grains (Davis & Greenstein 1951). This large-scale alignment can be seen in the polarization maps of Mathewson & Ford (1970), shown in Figure 1.10. Serkowski et al. (1975) determine empirically that stars for which interstellar polarization dominates will have a distinctive spectrum of polarization versus wavelength:

$$\frac{P(\lambda)}{P_{\max}} = \exp\left[-1.15\ln^2\left(\frac{\lambda_{\max}}{\lambda}\right)\right]. \tag{1.6}$$

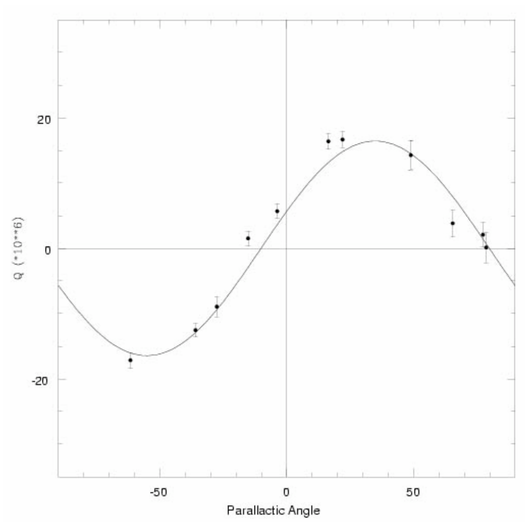

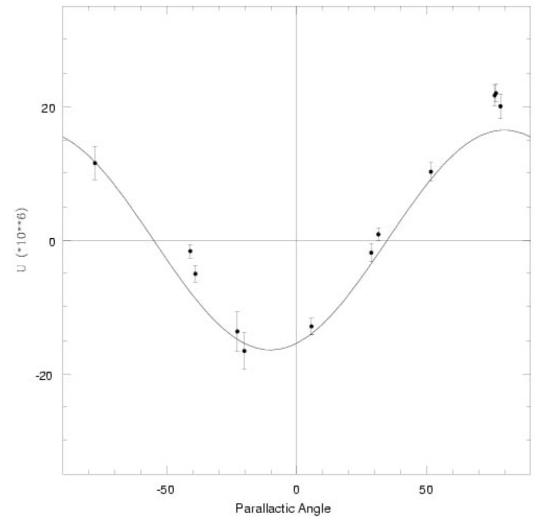

Figure 1.9: Telescope polarization of the 4.2-m William Herschel Telescope in La Palma, Spain, which is found to be $(16.4 \pm 0.4) \times 10^{-6}$. These plots are reproduced from Figure 6 of Hough et al. (2006b) by permission of PASP and the University of Chicago Press.

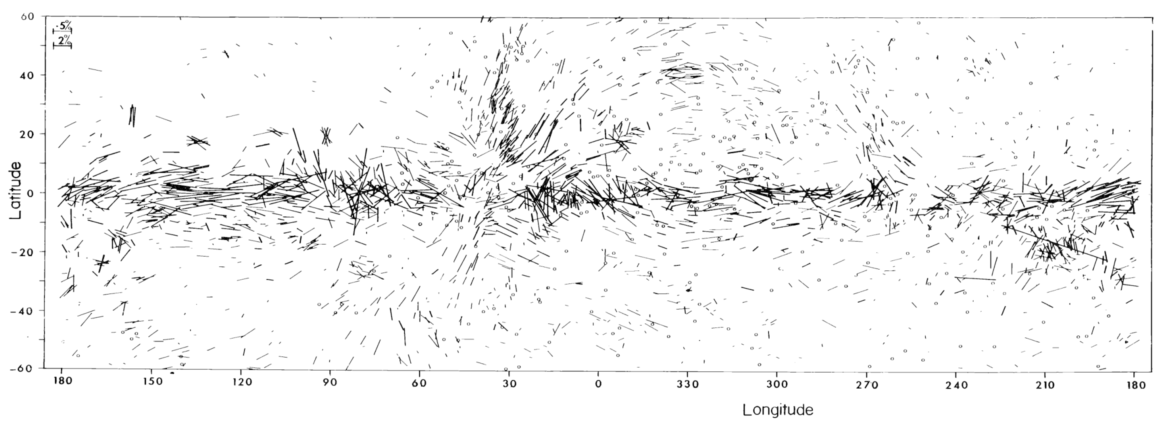

Figure 1.10: Interstellar polarization aligned to the galactic magnetic field, from Figure 1 of Mathewson & Ford (1970).

Here, $P_{\max}$ is the maximum polarization as a function of wavelength and $\lambda_{\max}$ is the wavelength of maximum polarization (Figure 1.11). Wilking et al. (1980) refined this relation further:

$$\frac{P(\lambda)}{P_{\max}} = \exp\left[-1.7\lambda_{\max}\ln^2\left(\frac{\lambda_{\max}}{\lambda}\right)\right]. \tag{1.7}$$

The empirical relation of Serkowski et al. (1975) is predicted by the model of interstellar dust proposed by Li & Greenberg (1997). They model dust as cylinders with length to diameter ratio of two, which consist of a silicate core and an organic, refractory mantle. Indeed, Figure 1.12 shows a comparison between polarization predicted by such grains (solid line) and observed interstellar polarization (dotted line). The inset illustrates the prediction of the Li & Greenberg (1997) model of the circular polarization (dotted line) sign change at the wavelength of peak linear polarization (solid line), $\lambda = \lambda_{\max}$. Figure 1.13 shows the first observations of this effect by Kemp & Wolstencroft (1972).

Interstellar polarization represents a significant systematic effect that is difficult to calibrate. This is because observed polarization is the sum of the telescope, instrument, interstellar, and intrinsic polarization vectors. While telescope and instrument polarization may be calibrated, calibration of interstellar polarization is less straightforward. Additionally, the degree of interstellar polarization increases with distance to the target (Figure 1.14) because of the increased number of dust grains in the line of sight column (Mathewson & Ford 1970, Barrett 1996, Fosalba et al. 2002). Therefore, interstellar polarization is significant for almost all targets of interest. For imaging polarimetry, and other relatively low precision polarimetric investigations, one can consult polarization maps to determine the degree and position angle of polarization for stars near the target (Figure 1.10). The mean interstellar polarization in the neighborhood of the target can then be subtracted from the observed polarization of the target.

Four types of observations are generally used to separate the interstellar and intrinsic components of observed polarization: polarization versus wavelength, rotation of position angle with wavelength, circular polarization, and temporal variability. For objects whose polarization spectrum differs from the Serkowski et al. (1975) relation, it is likely that the difference is due to intrinsic polarization of the source. The wavelength of peak polarization $\lambda_{\max}$ is comparable to the mean grain size along

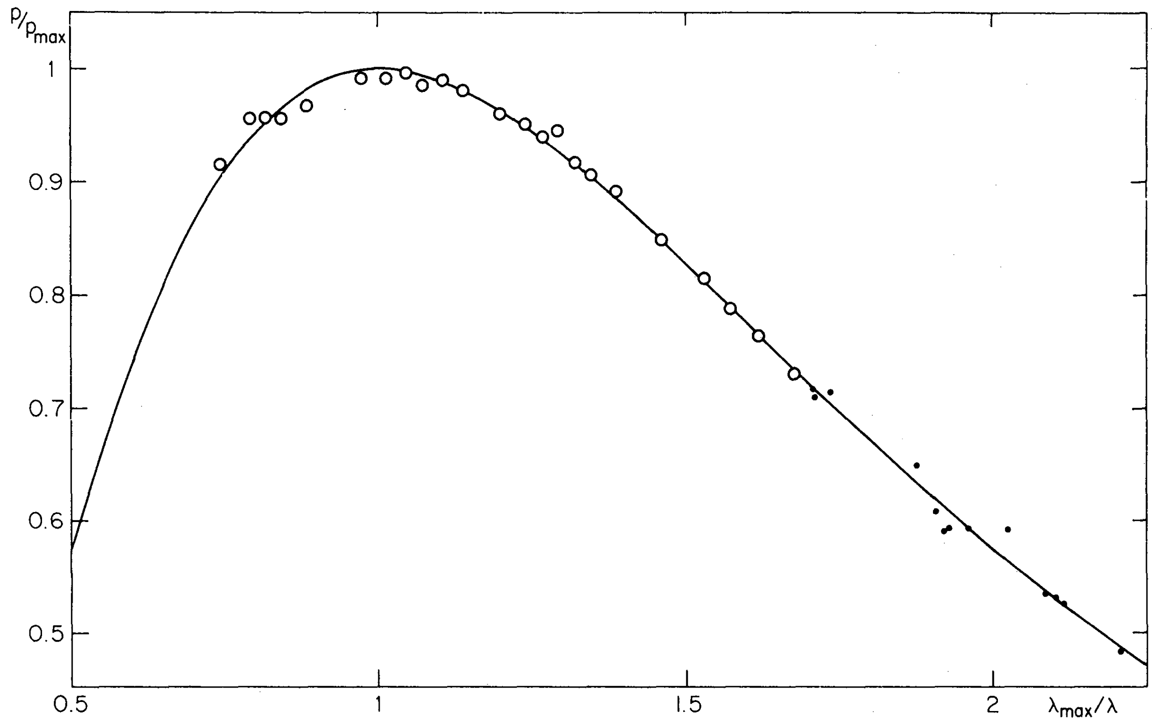

Figure 1.11: Empirical wavelength dependence of interstellar polarization from Equation 1.6. This figure is taken from Figure 3 of Serkowski et al. (1975).

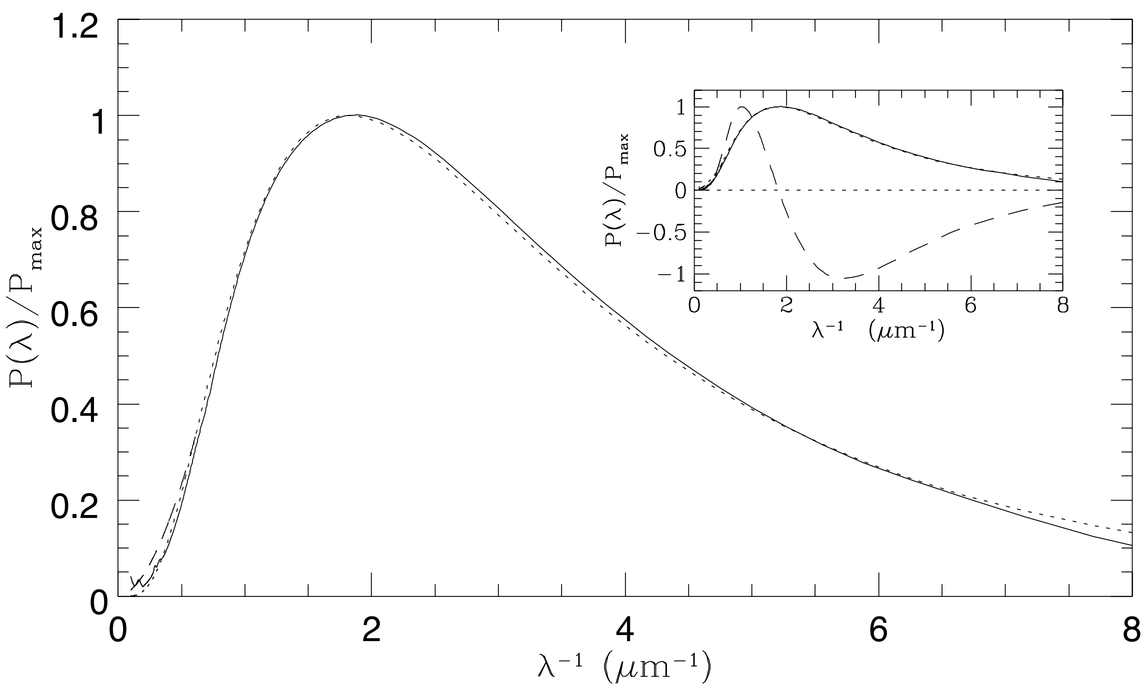

Figure 1.12: Theoretical wavelength dependence of interstellar polarization from Figure 4 of Li & Greenberg (1997). Note the agreement between theory (solid line) and observation (dotted line). The inset shows the reproduction of circular polarization (dashed line) sign change at the wavelength of linear polarization (solid line) maximum, $\lambda = \lambda_{\max}$.

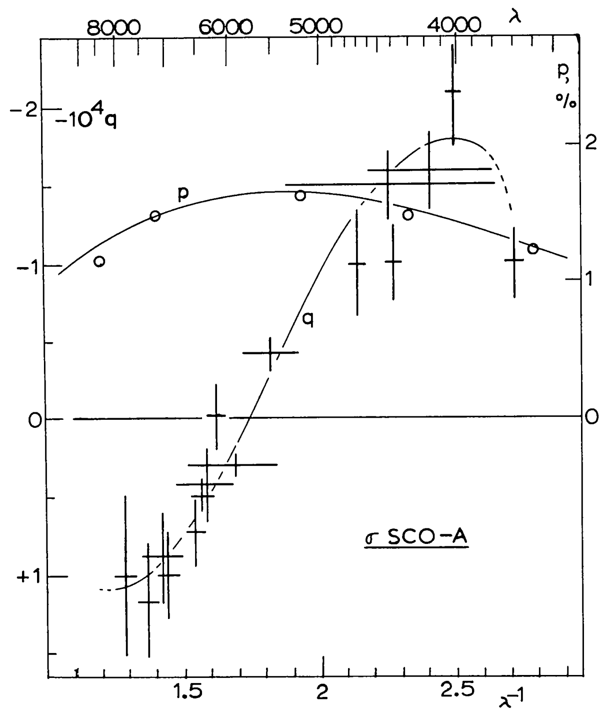

Figure 1.13: Observed circular polarization sign change near $\lambda = \lambda_{\mathrm{max}}$, labeled q, from Figure 1 of Kemp & Wolstencroft (1972). Linear polarization data, labeled p, are from Coyne & Gehrels (1966).

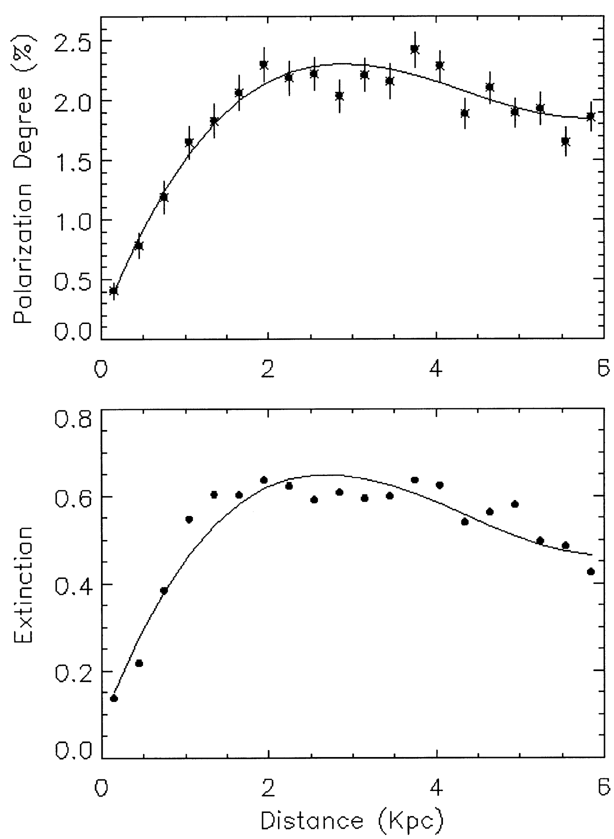

Figure 1.14: Increase in degree of interstellar polarization up to $d \approx 2$ kpc. Note the correlation of polarization with extinction. This figure is from Figure 3 of Fosalba et al. (2002).

the line of sight to the object. Therefore, if both grain size and orientation vary along the line of sight, the position angle of linear polarization will be a function of wavelength (Messinger et al. 1997, Whittet et al. 2001).

While both grain size and orientation must occur for interstellar polarization to generate a rotation of position angle with wavelength, only a change in grain orientation is required to generate circular polarization. This effect was predicted by van de Hulst (1957), and circular polarization of stars dominated by interstellar polarization was observed by Kemp (1972) and Kemp & Wolstencroft (1972). From theoretical modeling of polarization due to grains with varying orientation, Martin (1974) discovered that the handedness of interstellar circular polarization changes sign near the wavelength of peak linear polarization, confirming the observations of Kemp & Wolstencroft (1972).

Polarimetric variability of many stars is observed in high precision campaigns. It is assumed that variability on nightly timescales is indicative of intrinsic polarization, because the interstellar medium is not thought to be variable on those timescales. However, Walker (2007) observe lensing of the quasar Q0954+658 by an AU-sized, interstellar dust cloud $d \approx 500$ pc away from Earth (Figure 1.15). The timescale of this event is ≈ 100 days, with dramatic changes evident on a one week timescale. This shows that ISM variability is probably not important during an individual observing run, but it may be significant from run to run for strongly polarized sources.

Of the combination of the four types of observations listed above, polarimetric variability (linear, circular, or both) phase-locked to orbital or pulsational cycles is the strongest indicator of intrinsic polarization of the source. Additionally, deviation of polarization as a function of wavelength from Equation 1.6 indicates intrinsic polarization. For strongly polarized sources, with $P \approx 1\%$ or larger, rotation of polarimetric position angle with wavelength coupled with a lack of observed circular polarization may also indicate intrinsic polarization. This is because line of sight change in grain orientation is expected to convert linear polarization to circular polarization with $\approx 1\%$ efficiency (Martin 1974, Avery et al. 1975). Thus, intrinsic polarization of order 1% incident on a column of grains with varying orientation along the line of sight should generate detectable circular polarization of order one part in 10^4.

Lack of circular polarization towards such a target could imply intrinsic Rayleigh scattering.

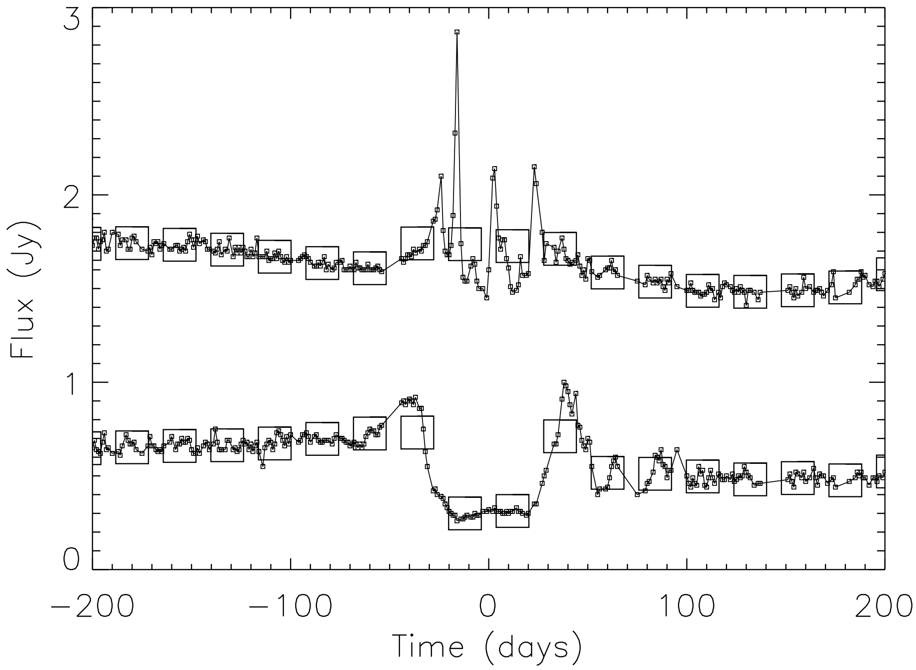

Figure 1.15: Scattering of quasar radio emission by an interstellar dust cloud. Boxes indicate binned observations over 24 day intervals. Top curve represents high frequency (8.1 GHz) observations, to which a 1 mJy vertical offset was applied. Bottom curve shows low frequency (2.7 GHz) monitoring of the event. Reprinted by permission from Walker (2007), Figure 2.

Rayleigh scattering occurs in neutral gas, which may be present in cool stars and accretion streams (Mason et al. 1974, Kallman & White 1982, White et al. 1983, Kitamoto et al. 1984). However, the gas density in the ISM is not significant to provide Rayleigh scattering of background starlight. The position angles of the intrinsic and interstellar polarization components will be different, so the superposition of intrinsic, Rayleigh scattering ($P \propto \lambda^{-4}$) and interstellar polarization (Equations 1.6 and 1.7) will cause a rotation of position angle with wavelength. For comparable degree of polarization between both components, the blue end of the optical spectrum will be dominated by intrinsic polarization while the red end will be dominated by interstellar polarization.

Conversely, the presence of circular polarization with a magnitude much higher than 1% of the degree of linear polarization implies an intrinsic source of circular polarization. Strong magnetic fields are thought to be the cause of such intrinsic circular polarization. This effect has been observed in Cepheid variables (Rudy & Kemp 1978) as well as in the high mass X-ray binary Cygnus X-1 (Michalsky et al. 1975a, b; Severny & Kuvshinov 1975; Michalsky & Swedlund 1977).

It is difficult to determine whether polarization of weakly polarized objects is intrinsic or due to interstellar polarization, which is one of the major pitfalls of polarimetry. As will be seen later, I determine the position angle of net polarization of the γ Oph debris disk to be aligned with the major axis of the disk as observed by Spitzer. This is clear evidence for intrinsic polarization of the disk. Since geometric information about circumstellar disks is of great importance for star, disk, and planet formation/evolution scenarios, polarimetry is necessary to understand these objects. However, the role of interstellar polarization in the neighborhood of such objects is not always clear, and this can limit the contribution expected of polarimetry.

1.3.3 Intrinsic Polarization Variability

The hot Jupiter parent stars τ Boö (Walker et al. 2008), HD 179949 (Shkolnik et al. 2005, Shkolnik et al. 2007), and HD 189733 (Hébrard & Lecavelier des Etangs 2006, Croll et al. 2007, Winn et al. 2007, Pont et al. 2007, Shkolnik et al. 2007, Moutou et al. 2008) are known to have significant starspot activity, and some spots appear to corotate with the planet. Since starspots are associated with magnetic field activity, it is likely that they induce polarimetric variability at the orbital frequency. This has been observed in τ Boö with PlanetPol, where the planetary signal appears to be swamped by polarized starspots (Hough et al. 2006a). While observations both on and off spectral features may distinguish between starspots and the planet (Figure 1.5), the reduction in throughput will decrease the precision of the measurement. Thus, observations of light scattered by hot Jupiters likely requires 10-m class telescopes or larger.

The lack of true phase-locking observed in Cygnus X-1 (Wolinski et al. 1996) and other OB supergiant/compact object binaries (Dolan & Tapia 1984, 1988) is due to stochastic variability in the system. This may hamper accurate measurement of the orbital inclination with polarimetry. Indeed, it appears that co-adding the modulation from many orbits may not produce the mean state of the system. Thus, single-orbit observations may be necessary, which reduces the polarimetric precision that can be attained. As a proof of concept of the polarimetric technique, I commissioned a polarimeter on the Hale 5-m telescope. The goal of this instrument was to observe and characterize the polarimetric modulation of the Cygnus X-1 high mass X-ray binary. The next chapter describes the engineering and initial results from the instrument.

References

Avery, R. W., Stokes, R. A., Michalsky, J. J., & Ekstrom, P. A. 1975, AJ 80, 1026.

Barrett, P. 1996, PASP 108, 412.

Bieging, J. H., Schmidt, G. D., Smith, P. S., & Oppenheimer, B. D. 2006, ApJ 39, 1053.

Charbonneau, D., Brown, T. M., Latham, D. W., & Mayor, M. 2000, ApJ 529, L45.

Coyne, G. V. & Gehrels, T. 1966, AJ 71, 355.

Croll, B., Matthews, J. M., Rowe, J. F., Gladman, B., Miller-Ricci, E., Sasselov, D., Walker, G. A. H., Kuschnig, R., Lin, D. N. C., Guenther, D. B., Moffat, A. F. J., Rucinski, S. M., & Weiss, W. W. 2007, ApJ 671, 2129.

Davis, L., Jr. & Greenstein, J. L. 1951, ApJ 114, 206.

Deming, D., Seager, S., Richardson, L. J., & Harrington, J. 2005, Nature 434, 740.

Dolan, J. F. & Tapia, S. 1984, A&A 139, 249.

Dolan, J. F. & Tapia, S. 1988, A&A 202, 124.

Fosalba, P., Lazarian, A., Prunet, S., & Tauber, J. A. 2002, ApJ 564, 762.

González Delgado, D., Olofsson, H., Schwarz, H. E., Eriksson, K., Gustafsson, B., & Gledhill, T. 2003, A&A 399, 1021.

Graham, J. R., Kalas, P. G., & Matthews, B. C. 2007, ApJ 654, 595.

Grinin, V. P. 1994, in The Nature and Evolutionary Status of Herbig Ae/Be stars, ed. P. S. Thé, M. R. Pérez, & E. P. J. van den Heuvel, ASP Conf. Ser., 62, 63.

Grinin, V. P., Thé, P. S., de Winter, D., Giampapa, M., Rostopchina, A. N., Tambovtseva, L. V., van den Ancker, & M. E. 1994, A&A 292, 165.

Hall, J. S. & Riley, L. A. 1976, Icarus 29, 231.

Hébrard, G. & Lecavelier des Etangs, A. 2006, A&A 445, 341.

Henson, G. D., Kemp, J. C., & Kraus, D. J. 1985, PASP 97, 1192.

Hough, J. H., Lucas, P. W., & Bailey, J. A. 2006a, in IAU Symp. 232, The Scientific Requirements of Extremely Large Telescopes, ed. P. Whitelock, B. Leibundgut, & M. Dennefeld (Cambridge: Cambridge Univ. Press), 350.

Hough, J. H., Lucas, P. W., Bailey, J. A., Tamura, M., Hirst, E., Harrison, D., & Bartholomew-Biggs, M. 2006b, PASP 118, 1302.

Johnson, J. J. & Jones, T. J. 1991, AJ 101, 1735.

Kallman, T. R. & White, N. E. 1982, ApJ 261, L35.

Kemp, J. C. 1972, ApJ 175, L35.

Kemp, J. C. & Wolstencroft, R. D. 1972, ApJ 176, L115.

Kitamoto, S. & Miyamoto, S. 1984, PASJ 36, 731.

Konacki, M. & Wolszczan, A. 2003, ApJ 589, 495.

Knutson, H. A., Charbonneau, D., Allen, L. E., Fortney, J. J., Agol, E., Cowan, N. B., Showman, A. P., Cooper, C. S., & Megeath, S. T. 2007, Nature 447, 183.

Li, A. & Greenberg, J. M. 1997, A&A 323, L566.

Lovis, C., Mayor, M., Francesco, P., Yann, A., Benz, W., Bouchy, F., Correia, A. C. M., Laskar, J., Mordasini, C., Queloz, D., Santos, N. C., Udry, S., Bertaux, J.-L., & Sivan, J.-P. 2006, Nature 441, 305.

Magalhães, A. M., Coyne, G. V., Codina-Landaberry, S. J., & Gneiding, C. 1986, A&A 154, 1.

Martin, P. G. 1974, ApJ 187, 461.

Mason, K. O., Hawkins, F. J., Sanford, P. W., Murdin, P., & Savage, A. 1974, ApJ 192, L65.

Mathewson, D. S. & Ford, V. L. 1970, Mem. RAS 74, 139.

Mayor, M. & Queloz, D. 1995, Nature 378, 355.

Messinger, D. W., Whittet, D. C. B., & Roberge, W. G. 1997, ApJ 487, 314.

Michalsky, J. J. & Swedlund, J. B. 1977, ApJ 212, 221.

Michalsky, J. J., Swedlund, J. B., & Avery, R. W. 1975a, Nature 254, 39.

Michalsky, J. J., Swedlund, J. B., & Stokes, R. A. 1975b, ApJ 198, L101.

Moutou, C., Donati, J.-F., Savalle, R., Hussain, G., Alecian, E., Bouchy, F., Catala, C., Collier Cameron, A., Udry, S., & Vidal-Madjar, A. 2008, arXiv:0707.2016.

Oudmaijer, R. D., Palacios, J., Eiroa, C., Davies, J. K., de Winter, D., Ferlet, R., Garzón, F., Grady, C. A., Cameron, A., Deeg, H. J., Harris, A. W., Horne, K., Merín, B., Miranda, L. F., Montesinos, B., Mora, A., Penny, A., Quirrenbach, A., Rauer, H., Schneider, J., Solano, E., Tsapras, Y., & Wesselius, P. R. 2001, A&A 379, 564.

Pont, F., Gilliland, R. L., Moutou, C., Charbonneau, D., Bouchy, F., Brown, T. M., Mayor, M.; Queloz, D., Santos, N., & Udry, S. 2007, A&A 476, 1347.

Raveendran, A. V. & Rao, N. K. 1989, A&A 215, 63.

Rudy, R. J. & Kemp, J. C. 1978, MNRAS 183, 595.

Schmid, H. M., Joos, F., & Tschan, D. 2006, A&A 452, 657.

Serkowski, K., Mathewson, D. S., & Ford, V. L. 1975, ApJ 196, 261.

Severny, A. B. & Kuvshinov, V. M. 1975, ApJ 200, L13.

Shkolnik, E., Walker, G. A. H., Bohlender, D. A., Gu, P.-G., & Kúrster, M. 2005, ApJ 622, 1075.

Shkolnik, E., Bohlender, D. A., Walker, G. A. H., & Collier Cameron, A. 2007, arXiv:0712.0004.

Stam, D. M., Hovenier, J. W., & Waters, L. B. F. M. 2004, A&A 428, 663.

Trammell, S. R., Dinerstein, H. L., & Goodrich, R. W. 1994, AJ 108, 984.

van de Hulst, H. C. 1957, *Light Scattering by Small Particles* (New York: Wiley).

Vink, J. S., Drew, J. E., Harries, T. J., Oudmaijer, R. D., & Unruh, Y. 2005, MNRAS 359, 1049.

Walker, M. A. 2007, ASP Conf. Ser. 365, 299.

Walker, G. A. H., Croll, B., Matthews, J. M., Kuschnig, R., Huber, D., Weiss, W. W., Shkolnik, E., Rucinski, S. M., Guenther, D. B., Moffat, A. F. J., & Sasselov, D. 2008, A&A 482, 691.

White, N. E., Kallman, T. R., & Swank, J. H. 1983, ApJ 269, 264.

Whittet, D. C. B., Gerakines, P. A., Hough, J. H., & Shenoy, S. S. 2001, ApJ 547, 872.

Wilking, B. A., Lebofsky, M. J., Kemp, J. C., Martin, P. G., & Rieke, G. H. 1980, ApJ 235, 905.

Winn, J. N., Holman, M. J., Henry, G. W., Roussanova, A., Enya, K., Yoshii, Y., Shporer, A., Mazeh, T., Johnson, J. A., Narita, N., & Suto, Y. 2007, AJ 133, 1828.

Wolinski, K. G., Dolan, J. F., Boyd, P. T., Biggs, J. D., Nelson, M. J., Percival, J. W., Taylor, M., & van Citters, G. W. 1996, ApJ 457, 859.

Wolszczan, A. & Frail, D. A. 1992, Nature 355, 145.

Yudin, R. V. & Evans, A. 2002, A&A 391, 625.